



RESEARCH ARTICLE

10.1029/2022AV000679

Regulation of the Respiration Quotient Across Ocean Basins

Allison R. Moreno¹ , Alyse A. Larkin² , Jenna A. Lee² , Skylar D. Gerace², Glen A. Tarran³ , and Adam C. Martiny^{1,2}

¹Department of Ecology and Evolutionary Biology, University of California Irvine, Irvine, CA, USA, ²Department of Earth System Science, University of California Irvine, Irvine, CA, USA, ³Plymouth Marine Laboratory, Plymouth, UK

Key Points:

- The respiration quotient ratios vary along latitudinal and meridional gradients
- A hierarchy of environmental conditions regulate the respiration quotient
- A varying oxygen-to-carbon remineralization ratio is important for connecting ocean biogeochemical cycles

Supporting Information:

Supporting Information may be found in the online version of this article.

Correspondence to:

A. C. Martiny,
amartiny@uci.edu

Citation:

Moreno, A. R., Larkin, A. A., Lee, J. A., Gerace, S. D., Tarran, G. A., & Martiny, A. C. (2022). Regulation of the respiration quotient across ocean basins. *AGU Advances*, 3, e2022AV000679. <https://doi.org/10.1029/2022AV000679>

Received 15 FEB 2022
Accepted 27 JUL 2022

Peer Review The peer review history for this article is available as a PDF in the Supporting Information.

Author Contributions:

Conceptualization: Allison R. Moreno, Adam C. Martiny
Data curation: Allison R. Moreno
Funding acquisition: Allison R. Moreno, Adam C. Martiny
Investigation: Allison R. Moreno
Methodology: Allison R. Moreno, Jenna A. Lee, Skylar D. Gerace, Glen A. Tarran
Supervision: Adam C. Martiny
Writing – original draft: Allison R. Moreno, Alyse A. Larkin, Adam C. Martiny
Writing – review & editing: Allison R. Moreno, Alyse A. Larkin, Jenna A. Lee,

Abstract A key uncertainty for predicting future ocean oxygen levels is the response and feedback of organic matter respiration demand. One poorly constrained component of the respiration demand is the oxygen-to-carbon remineralization ratio—the respiration quotient. Currently, multiple biological hypotheses can explain variation in the respiration quotient of organic matter produced in the surface ocean. To test these hypotheses, we directly quantified the particulate respiration quotient in 715 samples along a meridional section of the Atlantic Ocean and compared to previous Pacific Ocean observations. We demonstrate significant regional shifts in the respiration quotient and a two-basin average of 1.16. Possible diel oscillations were also observed in the respiration quotient. Basin and regional variation in the respiration quotient were positively linked to temperature, N versus P stress, and plankton size structure. These observations suggest a complex regulation of the respiration quotient with important implications for the regional coupling of carbon and oxygen cycling.

Plain Language Summary Decreasing ocean oxygen levels due to climate change have serious consequences for marine life. Biological oxygen demand is impacted by the respiration quotient, but the mean and regional variation of this key ocean biogeochemical parameter is still poorly understood. Using direct chemical measurements of particulate organic matter in multiple ocean basins, we test proposed hypotheses for how the respiration quotient is regulated. We show evidence that the respiration quotient changes systematically with a hierarchy of temperature, nutrient stress, and phytoplankton community structure. These observations imply that a varying respiration quotient can be an important driver of current and future ocean oxygen levels.

1. Introduction

Ocean observations suggest a decline in oxygen of more than 2% since 1960 (Schmidtko et al., 2017). In a 50-year time series within the eastern tropical North Atlantic and equatorial Pacific Oceans, declining oxygen and an expansion of the oxygen minimum zone ranging between 300 and 700 m deep have also been observed (Stramma et al., 2008). Finally, climate models predict increasing frequency of deoxygenation events and expansion of oxygen minimum zones (Bopp et al., 2013; Keeling et al., 2010). One major biological process influencing a decline in dissolved oxygen concentration is the respiration of organic matter produced by phytoplankton (Robinson, 2019). Whereas impacts from changes in the overall downward flux of organic matter and associated oxygen demand have received a lot of attention (DeVries & Deutsch, 2014; Falkowski et al., 2011; Keeling et al., 2010; Quay et al., 2020), we know less about the impact of changes to the oxygen-to-carbon remineralization ratio or the respiration quotient. The respiration quotient, $r_{-O_2:C}$, links the interior ocean cycles of carbon and oxygen and is defined as the amount of oxygen required to oxidize particulate organic matter (POM):



$$r_{-O_2:C} = \frac{\left(x + \frac{1}{4}z\right)}{x}, \quad (2)$$

where z signifies the oxidation state of the organic matter particularly seen in the concentration of hydrogen ions. An additional oxygen demand due to nitrification:



© 2022. The Authors.

This is an open access article under the terms of the [Creative Commons Attribution License](#), which permits use, distribution and reproduction in any medium, provided the original work is properly cited.

Skylar D. Gerace, Glen A. Tarran, Adam C. Martiny

yielding the total respiration quotient ($r_{\Sigma-O_2:C}$) describing the full oxidation of POM:

$$r_{\Sigma-O_2:C} = \frac{\left(x + \frac{1}{4}z + 2y\right)}{x}. \quad (4)$$

$r_{-O_2:C}$ is a fundamental driver of subsurface oxygen concentrations, with a resulting impact on denitrification rates in the ocean (Altabet, 2007; Karl & Grabowski, 2017). Earth System model simulations estimate a near linear relationship between $r_{-O_2:C}$ and the global ocean oxygen content, water column denitrification, and productivity (Moreno et al., 2020). Although we are starting to identify the importance of $r_{-O_2:C}$, we know less about the environmental regulation and regional variation.

Several hypotheses have been proposed to explain regional and short-term variation in the respiration quotient. In the eastern Pacific Ocean, the highest average values were observed in warm tropical regions (mean $r_{-O_2:C} = 1.19$), whereas the lowest values were found south of the subtropical front (mean $r_{-O_2:C} = 0.99$; Moreno et al., 2020). In addition, there was a lot of variation at small spatio-temporal scales. The observed changes in $r_{-O_2:C}$ have led to four potential hypotheses regarding the respiration quotient control. The first hypothesis is that temperature somehow regulates $r_{-O_2:C}$, but the exact biochemical mechanism is not clear. The second hypothesis is that daily partitions in photosynthesis, C storage, and respiration leads to short-term variations in the cellular chemical composition and $r_{-O_2:C}$ (Matallana-Surget et al., 2014; Van Mooy et al., 2002). The third hypothesis suggests that the intensity and type of nutrient stress regulate the cellular lipid content and respiration quotient. Nitrogen and to a lesser extent phosphorus limitation can induce lipid accumulation in the form of storage fats in many microalgae (Chen et al., 2015; Illman et al., 2000; Reitan et al., 1994). Thus, especially N stress may increase the production of reduced lipid carbon raising the respiration quotient. The fourth hypothesis is that variation in $r_{-O_2:C}$ is linked to an allometric scaling of membrane lipids to more oxidized cytoplasmic carbohydrates and proteins (Finkel et al., 2016). An extension of this hypothesis is that communities dominated by small phytoplankton, such as *Prochlorococcus*, compared to those with many eukaryotes will have a higher respiration quotient. It is worth noting that these hypotheses do not have to be mutually exclusive. Thus, several hypotheses exist for the regulation of the respiration quotient, but the relative importance of each is not yet determined.

Nutrient limitation type varies considerably within and between major ocean basins. Spatially, the Atlantic Ocean have highly dynamic nutrient regimes. Based on genomic biomarkers, the Atlantic compared to the eastern Pacific Ocean has higher nutrient stress diversity with strong gradients in both macro- and micro-nutrient stress (Ustick et al., 2021). The Atlantic Ocean has less upwelling and a higher iron supply compared to the eastern Pacific Ocean. Lower rates of upwelling results in faster macronutrient depletion, in addition to higher rates of N fixation, causing widespread phosphorus limitation in especially the northern part of the Atlantic Ocean (Moore et al., 2013; Ustick et al., 2021). Due to differences in nutrient limitation, latitudinal shifts in the respiration quotient in the Atlantic versus Pacific Ocean are unknown. However, a comparison between the two-ocean basins would allow us to test the hypotheses presented above. For example, the wide P-limited region in the North Atlantic Ocean (Mather et al., 2008) could lead to a lower respiration quotient compared to N-stressed regions in the eastern Pacific Ocean. Furthermore, the absence of strong upwelling in the central Atlantic but elevated temperature would help separate the relative impact of nutrient stress versus temperature. Thus, a detailed quantification of $r_{-O_2:C}$ across the Atlantic Ocean combined with our previous observations from the Pacific Ocean may enable us to further disentangle the regulation of the respiration quotient.

In this study, we will address the following research questions: (a) What is the average and regional variation of $r_{-O_2:C}$ across a wide latitudinal and environmental gradient in the Atlantic Ocean and (b) which of our four hypotheses can best explain the observed variation in $r_{-O_2:C}$?

2. Materials and Methods

2.1. Sample Collection

Seawater samples were collected during Atlantic Meridional Transect 28 (AMT28) cruise aboard the Royal Research Ship James Clark Ross from 23 September to 29 October 2018, between 49° 38.3' N, 5° 30.1' W off the UK to 46° 1.0' S, 49° 52.3' W near the Falkland Islands. Seawater for particulate organic carbon (POC) and nitrogen, and chemical oxygen demand were vacuum-filtered from the onboard underway system. The underway

intake was located at a depth of ~5 m from the sea surface. All carboys were rinsed twice with underway seawater before sampling took place. Non-replicate samples for POC:N and particulate chemical oxygen demand (PCOD) were taken hourly. At noon, triplicate samples for POC:N and PCOD were taken and averaged. Our sampling plan was designed to capture diel cycling. Water was passed through a 30 μm nylon mesh (Small Parts #7050-1220-000-12) to remove large particles from the sample. Samples were collected on pre-combusted 500°C GF/F filters (Whatman, GE Healthcare, Little Chalfont, Buckinghamshire, UK) for the analysis of particulate organic C and N and chemical oxygen demand. Sample volume was determined on a per station basis, ranging from 3 to 8 L. All filters were then folded in half, sealed inside pre-combusted aluminum foil, and stored at -20°C until analysis.

2.2. Particulate Organic Carbon

POC samples were dried at 55°C (24 hr) and then stored in a desiccator with concentrated HCl fumes for 24 hr to remove inorganic carbonates. The filters were then dried for 48 hr at 55°C before being folded and pelletized into tin capsules (CE Elantech, Lakewood, New Jersey). The tin capsules are then analyzed on a Flash EA 1112 NC Soil Analyzer (Thermo Scientific, Waltham, Massachusetts) against blank filters, an atropine ($\text{C}_{17}\text{H}_{23}\text{NO}_3$) and acetanilide ($\text{C}_8\text{H}_9\text{NO}$) standard curve.

2.3. Particulate Chemical Oxygen Demand Assay

PCOD samples were quantified following Moreno et al. (2020). Samples were removed from their foil packets and placed in petri dishes at 50°C for 24 hr. Filters were then transferred to HACH HR+ COD vials (Product no. 2415915 containing mercuric sulfate). Two mL of Milli-Q water was added to each vial and inverted to submerge the filters completely. Vials were digested at 150°C for 2 hr. Samples were then cooled to room temperature. Due to uneven precipitation occurring, precipitation was induced by adding 92.1 μL of 0.17 M (9.5 g l^{-1}) NaCl to each vial. Vials were inverted twice and centrifuged for 30 min at 2,500 rpm and read on a photo-spectrometer at a wavelength of 600 nm. Note: dichromate does not oxidize organic nitrogen, so this assay only quantifies changes in the carbon oxidation state. To quantify PCOD, in $\mu\text{M O}_2$, we utilize a standard curve based on HACH certified COD 1,000 mg/L standard stock solution (Product no. 2253929). To determine our filters have no impact on sample quantification and to follow methodology from Moreno et al. (2020), we test blank filters with a standard curve.

2.4. $r_{-O_2:C}$ Ratio

The $r_{-O_2:C}$ ratios were taken from the mean concentrations of PCOD and POC. We compare our measured $r_{-O_2:C}$ ratio to that of Redfield at 1 (Redfield, 1958) and Anderson's predicted value of 1.1 (Anderson, 1995). Both comparison values are estimated based on the nitrogen oxidized to ammonium. The standard deviation for $r_{-O_2:C}$ were calculated as a pooled sample:

$$\sigma_{r_{-O_2:C}} = \frac{-O_{2,aver}}{C_{aver}} \times \sqrt{\left(\left(\frac{\sigma_{-O_2}}{-O_{2,aver}}\right)^2 + \left(\frac{\sigma_C}{C_{aver}}\right)^2\right)}$$

2.5. Cell Size Ratio

Flow cytometry samples were taken from CTD casts during the Atlantic Ocean (AMT28) cruise track in clean 250 mL polycarbonate bottles. Samples were collected from surface to 200 m deep from predawn and solar noon casts. Samples were measured using a Becton Dickinson FACSsort flow cytometer to characterize and count *Prochlorococcus*, *Synechococcus*, and pico- and eukaryote phytoplankton. Separate samples were fixed with glutaraldehyde solution (sigma-Aldrich, 50%, Grade 1 0.5% final concentrations, 30 min at 4°C) within half an hour of surfacing. Samples were stained for 1 hr at room temperature in the dark with SYBR Green I. Samples were generally analyzed within 3 hr utilizing the Becton Dickinson FACSsort flow cytometer to characterize and count bacterioplankton. All abundance estimates were recorded as cells mL^{-1} . Cellular abundance was converted to carbon content based on Table 1.

Table 1
Carbon Content Per Plankton Cell

Plankton type	Conversion factor (fg C/cell)	Standard deviation (fg C/cell)	Source
<i>Prochlorococcus</i>	50	14	Casey et al. (2013)
<i>Synechococcus</i>	255	50	Casey et al. (2013)
Picoeukaryotes	768	28	Linacre et al. (2010)
Heterotrophic bacteria (low and high DNA content)	20	5	Casey et al. (2013)
Nano-eukaryotes	8,892	2,964	Linacre et al. (2010)
Cryptophytes	8,892	2,964	Linacre et al. (2010)
Coccolithophores	8,892	2,964	Linacre et al. (2010)

Note. Used to convert cell counts to carbon content per ml.

We calculate the small-to-large cell size ratio as follows:

$$C = \frac{\text{pro} \times \left(50 \frac{\text{fgC}}{\text{cell}}\right) + \text{syn} \times \left(255 \frac{\text{fgC}}{\text{cell}}\right) + (\text{HBlow} + \text{HBhigh}) \times \left(20 \frac{\text{fgC}}{\text{cell}}\right)}{\text{Pico} \times \left(768 \frac{\text{fgC}}{\text{cell}}\right) + (\text{Nano} + \text{Cryp} + \text{Cocco}) \times \left(8,892 \frac{\text{fgC}}{\text{cell}}\right)}$$

Using a Monte Carlo approach, we estimate a 95% confidence interval around the small-to-large size ratio. This was done by first constructing a normal distribution, based on the mean and standard deviation, for each plankton type. Then we randomly chose a conversion factor for each type and estimate the ratio. From the 1,000 runs, we estimated the 95% confidence interval. Following the calculation of small-to-large cell size ratio for all depths, we conducted a linear interpolation of surface samples, ranging in depth from 5 to 13 m, to match the number of POM samples, $n = 715$, taken along AMT28.

2.6. Cellular Stress Index

Nutrient stress indexes were obtained from Ustick et al. (2021). The nutrient stress index (high P stress, Ω_{Ph} , and high N stress Ω_{Nh}) is an indicator of microbial adaptation in *Prochlorococcus* to nutrient availability. Once data was obtained from the authors, we performed a linear interpolation to match the number of POM samples taken along both cruise tracks (Pacific Ocean, $n = 198$ and Atlantic Ocean, $n = 715$).

2.7. Nutrient Parameters

Nutricline depth was chosen as a proxy for nutrient availability and was calculated based on a nitrate concentration of 1 μM . Nitrate and phosphate concentrations were analyzed using an Auto Analyzer on ship.

2.8. N^* Derivation

Deviation from Redfield nutrient concentrations (N^*) was calculated for a depth of 200 m as follows:

$$N_{200}^* = [\text{NO}_3]_{200}^{-1} - 16[\text{PO}_4]_{200}^{-3}$$

2.9. Statistical Analysis

All analyses were completed in MATLAB. Statistical nonlinear models were fitted using seven predictor variables (temperature [$^{\circ}\text{C}$], nutricline depth [$Z_{\text{NO}_3 = 1 \mu\text{M}}$], phosphate [μM], N_{200}^* , Ω_{Ph} , Ω_{Nh} , and cell size ratio [small to large phytoplankton]). R^2 and Akaike Information Criterion (AIC) were used to compare across models. For all regressions containing interpolated parameters, a random sampling of cruise data was conducted to ensure results were not bias.

For estimating a baseline DOM adsorbed to our GF/F filters, we apply a volume-regression. Utilizing previous marine samples (Moreno et al., 2020), we fit a regression curve over four volumes of samples. We interpret the intercept to be the concentration adsorbed to the filters alone. Following this, we can estimate the percentage of DOM on our filters.

For diel cycles identified, a sine function was added to the model with a fixed 24 hr period.

$$y = p(1)_y \times \sin\left(\frac{\text{Hrs} \times 2\pi}{24} + p(2)_y\right),$$

where $y = \text{POC}, \text{COD}, r_{-02:C}$. Residuals between observations and a 46 point moving average were used for comparing the diel cycling of POM and $r_{-02:C}$ ratio at each station.

Next, we conducted three principal component analyses (PCAs) for the respiration quotient in the Atlantic Ocean, Pacific Ocean, and combined data set. Each predicting parameter (temperature, PO_4 , $Z_{\text{NO}_3 = 1 \mu\text{M}}$, cell size, N_{200}^* , Ω_{ph} , and Ω_{Nh}) was normalized and scaled between 0 and 1 across all stations where parameters were available (Atlantic—612, Pacific—149, and combined—826). These parameters were used as inputs to each PCA ($n \times m$ matrix of n stations and m normalized parameter). We utilized a stepwise function to determine the combination of principal components (PCs) that best explained $r_{-02:C}$ variability (i.e., lowest AIC value).

3. Results

We quantified hydrographic conditions, phytoplankton community structure, POM, and the respiration quotient along an Atlantic Ocean latitudinal gradient. Samples ($n = 715$) were taken during the AMT28 cruise aboard the Royal Research Ship James Clark Ross from 23 September 2018 to 29 October 2018, between $49^\circ 38.3' \text{N}$, $5^\circ 30.1' \text{W}$ to $46^\circ 1.0' \text{S}$, $49^\circ 52.3' \text{W}$ (Figure S1 in Supporting Information S1). We used these observations to identify regional variability and diel cycling in $r_{-02:C}$ across the basin. Subsequently, we compared the respiration quotient between the Atlantic and Pacific Oceans to further understand the environmental regulation.

Temperature, macronutrient concentrations, and nutricline depth delineated eight Longhurst regions at the time of the cruise (Figure 1; Reygondeau et al., 2013). Sample collection began off the coast of Plymouth, UK in the Northeast Atlantic Shelves region (1:NECS) with an average temperature of 16.3°C and low surface macronutrients. The North Atlantic Drift (2:NADR) had temperatures of 16.7°C plus moderate levels of nitrate ($0.36 \mu\text{M}$) and phosphate ($0.11 \mu\text{M}$). The Northeast Atlantic subtropical gyre (3:NAST) had intermediate temperatures (23.1°C), a complete surface depletion of macronutrients, and a deepened nutricline. N^* (deviation from the Redfield ratio in nutrient concentrations) at 200 m depth (N_{200}^*) was generally positive within 3:NAST until $\sim 21^\circ\text{N}$ (Figure 1c). The North Atlantic tropical gyre region (4:NATR) had the highest average temperatures (27.0°C), depleted macronutrients (below detection limits), an intermediate nutricline depth of 80 m, and varying N_{200}^* . Although N_{200}^* varied within this region, it was at its most positive until $\sim 10^\circ\text{N}$ suggesting high N fixation in this part of the basin. The Western Tropical Atlantic region (5:WTRA) and the South Atlantic Gyre (6:SATL) had intermediate temperatures (23.6°C and 20.3°C), no measurable surface nutrients, and a deep nutricline. Additionally, we found the lowest N_{200}^* (-4.4) in 5:WTRA. The final two southern regions were the transitional South subtropical convergence (7:SSTC) region and the Southwest Atlantic shelves (8:FKLD). Here, temperature was low (10.2°C), surface macronutrients high ($6 \mu\text{M} \text{NO}_3$ and $0.6 \mu\text{M} \text{PO}_4$), and N_{200}^* of -2.6 . Thus, we detected a meridional gradient in environmental conditions as well as slight differences between each hemisphere.

POM concentrations were regionally variable and exhibited three local maxima (Figure 2). POC and PCOD concentrations were lowest in 5:WTRA and 6:SATL (POC: 1.3 and $1.6 \mu\text{M}$; PCOD: 1.6 and $2.0 \mu\text{M}$). POM concentrations were intermediate in 3:NAST (POC: $2.3 \mu\text{M}$ and PCOD: $2.7 \mu\text{M}$), and 4:NATR: (POC: $2.4 \mu\text{M}$ and PCOD: $2.8 \mu\text{M}$). In high latitude regions, (i.e., 1:NECS, 2:NADR and 7:SSTC), POM concentrations were high (POC: $8.8 \mu\text{M}$, $5.5 \mu\text{M}$, $5.4 \mu\text{M}$ and PCOD: $10.0 \mu\text{M}$, $6.0 \mu\text{M}$, $6.0 \mu\text{M}$). As such, POM concentrations were lowest in the South Atlantic subtropical gyre regions and elevated at high latitudes, and just north of the equator.

The respiration quotient showed clear latitudinal and regional variation across the Atlantic Ocean (Figure 2c). Generally, POC and PCOD were highly correlated ($r_{\text{Pearson}}^2 = 0.91$, $P < 0.0001$). The variation in $r_{-02:C}$ was symmetric upon the equator with a higher ratio near the equator and into the subtropical gyres and lower toward high latitudes (Figure 2c). In the Northern Hemisphere, 1:NECS had the lowest $r_{-02:C}$. In the South-

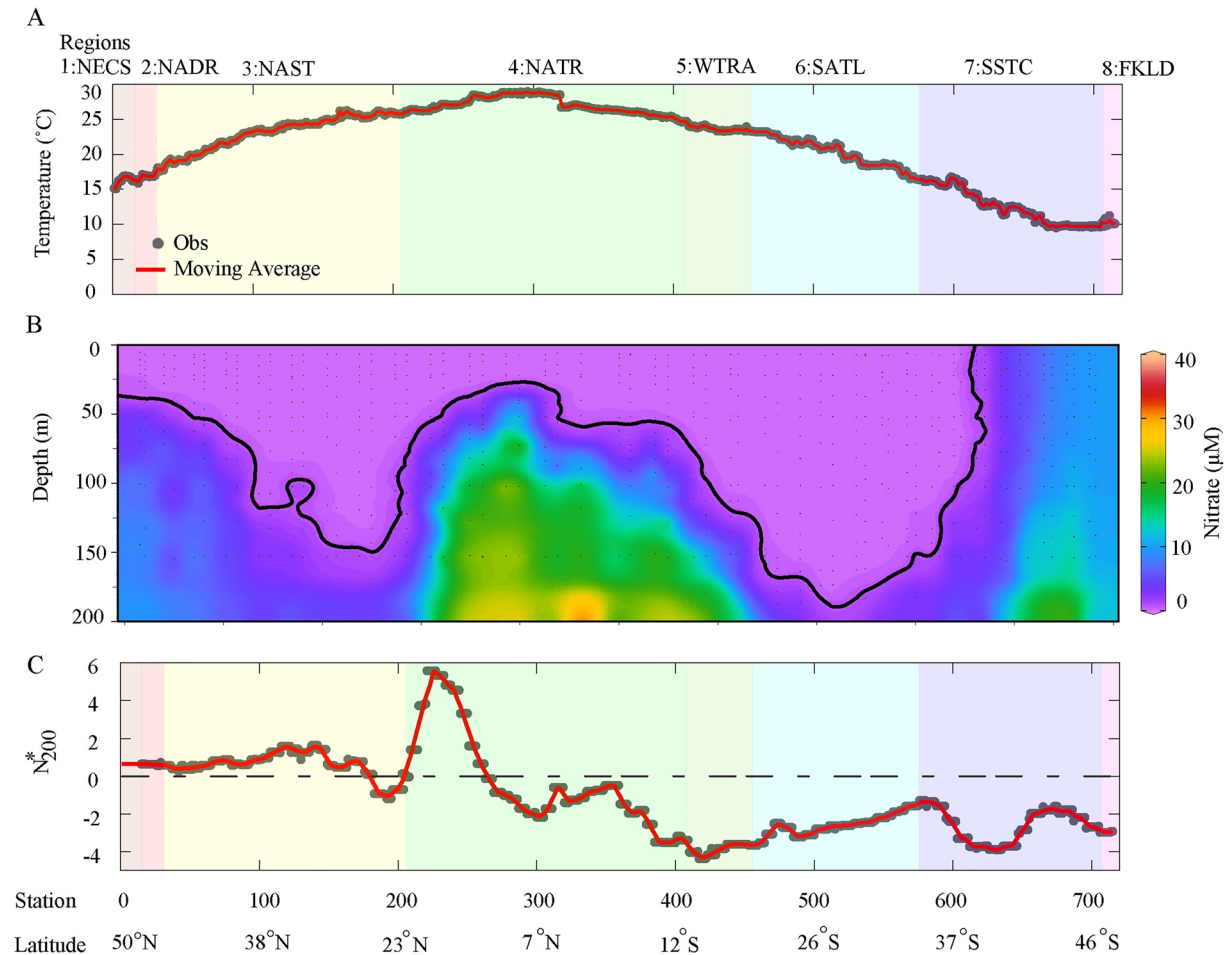


Figure 1. Regional variation in environmental conditions across the AMT28 section. (a) Sea surface temperature. (b) Nitrate concentration with the nutricline depth marked with the black line (where [Nitrate] is 1 μM). (c) N^* ($N^* = \text{NO}_3^- \text{Station, 200 m} - 16 \times \text{PO}_4^{3-} \text{Station, 200 m}$) at 200 m depth. A dashed dark gray line denotes the zero. Observations are marked as gray dots. The red line represents a 4-hr moving average. Colored background represents Longhurst regions labeled at the top of the figure. Regions are represented as follows: 1:NECS (Northeast Atlantic Shelves), 2:NADR (North Atlantic Drift), 3:NAST (Northeast Atlantic Subtropical Gyre), 4:NATR (North Atlantic Tropical Gyre), 5:WTRA (Western Tropical Atlantic), 6:SALT (South Atlantic Gyre), 7:SSTC (South Subtropical Convergence), and 8:FLKD (Southwest Atlantic Shelves).

ern Hemisphere, 5:WTRA (1.22) and 6:SATL (1.20) were statistically higher than 7:SSTC (1.12) and 8:FLKD (1.03). There was also a meridional skew in the warmer regions, whereby $r_{-O_2:C}$ was slightly lower in the northern compared to southern hemisphere (Figures 2c and 3). The average Atlantic Ocean-wide respiration quotient was $1.16^{1.93}_{0.75}$ (Figure 2c) and thus indistinguishable from the Pacific Ocean (Moreno et al., 2020) (Figure S2 in Supporting Information S1). However, the spread in the $r_{-O_2:C}$ between the two basins was statistically different (Kolmogorov-Smirnov test; Figure S2 in Supporting Information S1). Overall, we saw clear regional variation in the Atlantic, with the highest $r_{-O_2:C}$ near the equator, lowest in temperate biomes, and a difference between hemisphere (Figure 3).

We observed diel variability for each POM concentration and the respiration quotient (Figure S3 in Supporting Information S1). POC and PCOD showed strong daily oscillation. POC experienced a maximum at 21:00 and a minimum at 09:00 (sine function regression; p -value = 0.0004). PCOD displayed an approximate two-hour lag to POC (sine function regression; p -value = $1.26e-7$; Figure S3 in Supporting Information S1). Due to this lag, the respiration quotient diel cycle was not visually as strong, however, it does exhibit a maximum at 03:00 and a minimum near 15:00 (sine function regression; p -value = 0.0036). On average there was a change of $0.15 (\pm 0.03)$ in the respiration quotient over the course of the day.

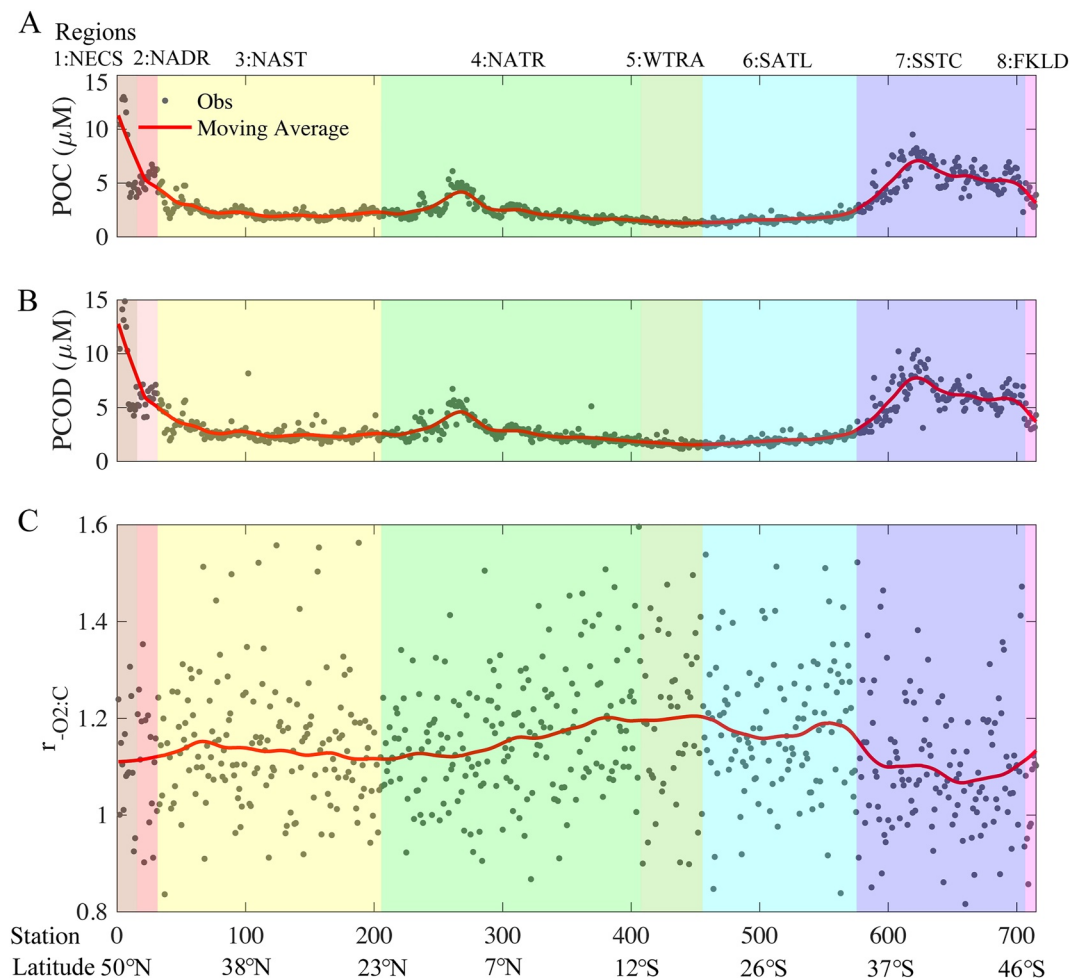


Figure 2. Particulate organic matter and respiration quotient along the Atlantic Ocean cruise track. (a) Surface particulate organic carbon. (b) Surface particulate chemical oxygen demand. (c) Surface molar respiration quotient. Observations are marked as gray dots. In panels (a) and (b), the red line represents a 48-hr moving average. In panel (c), the red line represents a 72-hr weighted moving average using *rlowess* in MATLAB. Colored background represents the different ocean subregions.

We first grouped environmental changes using a multi-dimensional PCA (Figure 4). Many environmental conditions and associated phytoplankton community structure show strong meridional changes. We explicitly accounted for this co-variance using principal components (PC) and linked each PC to variation in $r_{\text{-O}_2:\text{C}}$. The parameters used within the multi-dimensional analysis were environmental (temperature, phosphate, nutricline depth, and N_{200}^*) and biological (nutrient stress indexes and a cellular size ratio). Nutrient stress indexes for high P stress (Ω_{ph}) and high N stress (Ω_{Nh}) were retrieved from a metagenomic biomarker analysis (Ustick et al., 2021). Cell size is defined as a biomass-weighted cell size ratio of small (*Prochlorococcus*, *Synechococcus*, and heterotrophic bacteria) to larger (picoeukaryotes, nanoeukaryotes, cryptophytes, and coccolithophores) phytoplankton. In the Atlantic Ocean, our first principal component (PC1) represented the latitudinal gradient in environmental and biological conditions (i.e., positive with temperature, nutricline, overall nutrient stress, negative with nutrient concentrations, and smaller cells). PC2 captured the hemisphere shift in nutrient stress regimes. A negative PC2 corresponded to elevated P stress (Ω_{ph}) and N_{200}^* seen in the northern hemisphere, whereas a positive PC2 represented high Ω_{Nh} and a deeper nutricline seen in part of the southern hemisphere. A positive link between both PC1 and PC2 against $r_{\text{-O}_2:\text{C}}$ produced the best fit model (p -value = 4×10^{-7} ; AIC = -490) (Figure 4). Thus, our data analysis suggests that a meridional gradient in environmental conditions plus hemisphere shifts in N versus P stress contribute to variation in the respiration quotient.

A detailed comparison between Atlantic and Pacific Ocean observations supported that the respiration quotient was elevated in N compared to P-stressed regions (Figure 5). P stress was common in the North Atlantic Ocean

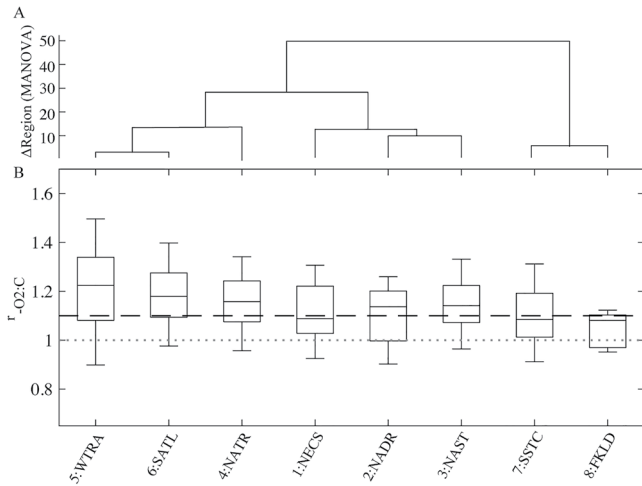


Figure 3. Atlantic regional difference in the respiration quotient. (a) Clustering of group means after a multivariate joint particulate organic carbon and particulate chemical oxygen demand analysis of variance (one-way MANOVA). (b) Regionally observed respiration quotients and comparisons to Redfield ($r_{-O_2:C} = 1.0$; dotted line; Redfield, 1958) and Anderson ($r_{-O_2:C} = 1.1$; dashed line; Anderson, 1995) theoretically predicted values.

but rare in both the South Atlantic and eastern Pacific Ocean (Figures 5a and 5b). N stress was less severe in the North Atlantic (except for the gyre core) and more widespread in both the South Atlantic and South Pacific Oceans. The hemisphere switch from P to N stress in North toward the South Atlantic Ocean corresponded to a higher $r_{-O_2:C}$. In further support, $r_{-O_2:C}$ was also higher in the N stressed eastern South Pacific subtropical gyre compared to the North Atlantic. Correlation analyses demonstrated that it can be challenging to identify the role of nutrient stress using individual transects (Figure 5c). However, the combined data from both the Atlantic and Pacific Ocean clearly suggested a higher respiration quotient under N compared to P stress.

The respiration quotient was only partially linked to the plankton community size structure. A biomass ratio of the small (*Prochlorococcus*, *Synechococcus*, and heterotrophic bacteria) to large (picoeukaryotes, nanoeukaryotes, cryptophytes, and coccolithophores) plankton was high in the subtropical gyres, at intermediate levels near the equator and lowest in the colder, nutrient-rich sections at higher latitudes (Figure 6). Thus, the cell size ratio was relatively symmetric upon the equator and showed limited hemisphere difference. In the South Atlantic, peaks in the small-to-large ratio corresponded to peaks in the respiration quotient (Figure 6). However, such a relationship between size structure and the respiration quotient was less clear in the northern hemisphere. In the region between the equator and $\sim 35^\circ N$, the cell size ratio peaked but the respiration quotient was low (Figure 6). Thus, although differences in phytoplankton cell size could be linked to the overall latitudinal gradient in the respiration quotient, the decoupling in the North Atlantic Ocean suggested only a partial control.

ences in phytoplankton cell size could be linked to the overall latitudinal gradient in the respiration quotient, the decoupling in the North Atlantic Ocean suggested only a partial control.

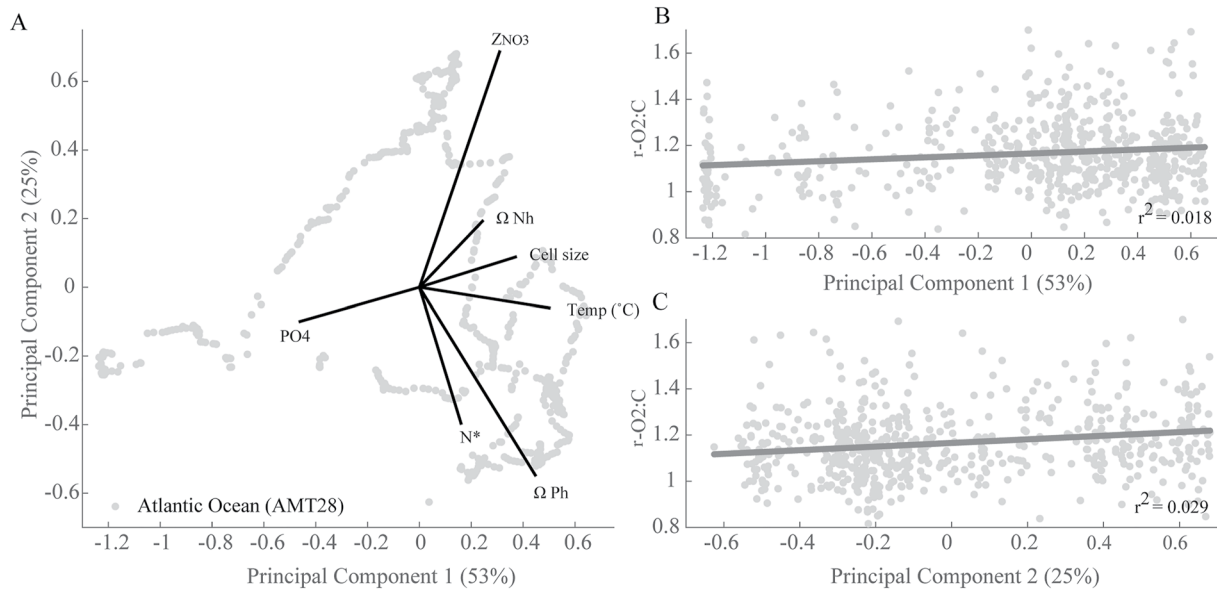


Figure 4. Principal component analysis (PCA) of environmental parameters for samples where the respiration quotient was taken along the Atlantic Ocean (AMT28) cruise track. (a) PCA of seven environmental variables (temperature, PO_4 , nutricline depth [Z_{NO_3}], N^* , cell size, P stress [Ω_{Ph}], and N stress [Ω_{Nh}]) at 612 stations. (b and c) $r_{-O_2:C}$ explained by the first and second principal component including the r^2 based on linear regression analysis. The percentages of total variance represented by principal components (PC) 1 and 2 are shown in parentheses. Gray dots represent PC scores for each station.

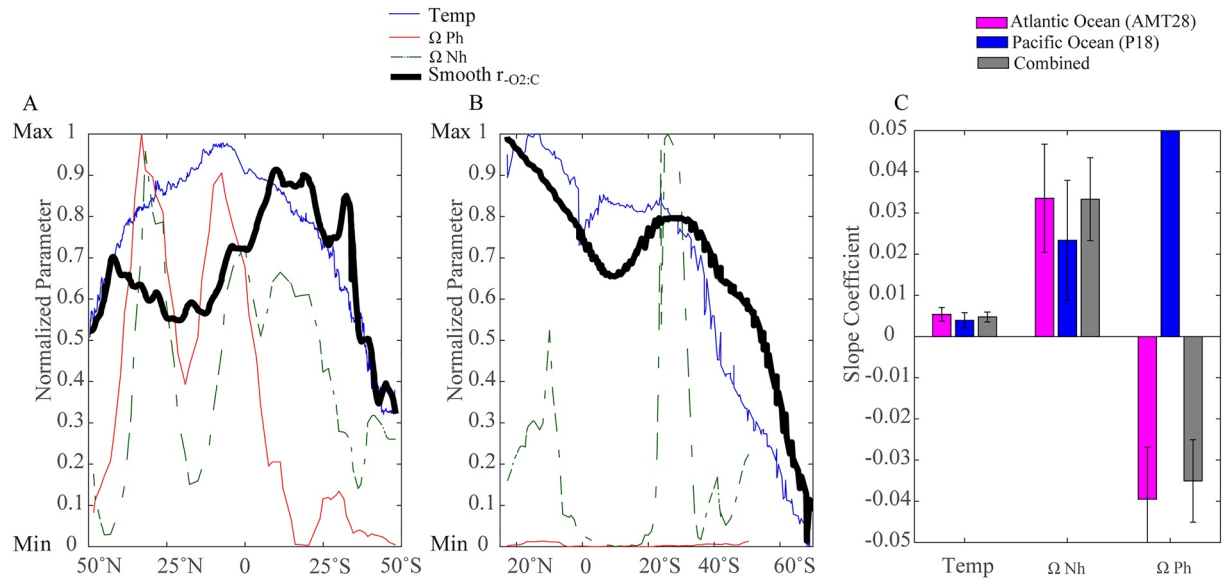


Figure 5. Link between nutrient stress type and the respiration quotient. (a) Atlantic Ocean (AMT28) cruise track. (b) Pacific Ocean (P18) cruise track. (c) Slope coefficients based on linear regression equation including temperature, Ω_{Ph} , and Ω_{Nh} . In panels (a and b) color lines represent normalized parameters where blue is temperature, red is phosphorus stress index (Ω_{Ph}), and a dashed green is nitrogen stress index (Ω_{Nh}). In panel (c) pink represents the Atlantic Ocean, blue represents the Pacific Ocean, and gray represents the combined data set. The slope coefficient is the linear slope coefficient value based on a linear regression test.

4. Discussion

The direct quantification of POM concentrations and the respiration quotient in the Atlantic Ocean allows us to estimate basin-specific patterns and test hypotheses regarding the environmental regulation. Our study provides evidence for a hierarchy of controlling factors for the respiration quotient across ocean basins. The primary control is a combination of temperature and overall nutrient availability, which in turn impacts the plankton community size structure. This results in a clear meridional gradient in the respiration quotient across both the Atlantic and Pacific Ocean. In an earlier study (Moreno et al., 2020), we speculated that smaller cells with a large membrane to cytosol biomass ratio would lead to more reduced carbon and a higher respiration quotient. Here, we

find partial support for this hypothesis and the associated latitudinal gradient (Figure 6). However, we also see that N compared to P stress promotes a higher respiration quotient. This response may be linked to the production and accumulation of storage lipids during N stress (Juneja et al., 2013; Reitan et al., 1994; Thompson et al., 1992). It is also possible that planktonic cells are either producing more oxidized carbohydrates or lessening their storage molecules during P stress (Van Mooy et al., 2006, 2009). Another factor to consider is the presence and fate of detrital POM captured on our filters and its influence on the respiration quotient. We primarily interpret variation in the respiration quotient via the biological regulation of cellular composition. However, a significant fraction of POM is “detrital” (Kaiser & Benner, 2008). This POM pool could contribute to the regulation of the respiration quotient if (a) there is a regional shift in the fraction of detrital matter to overall POM or (b) the composition of detrital matter changes. However, regional shifts of detrital matter are currently unknown. On the other hand, few studies have determined the differences in compositional makeup. One study found that up to 25% of POC pools are detrital matter and that particular molecular structures, such as peptidoglycan and peptides, are more present in POM versus DOM (Kaiser & Benner, 2008). Certain molecular classes may also be preferentially remineralized whereas others are enriched following microbial processing (Jiao et al., 2010; Wakeham et al., 1997). Hedges and co-workers saw divergent patterns when comparing organic matter in sediment traps

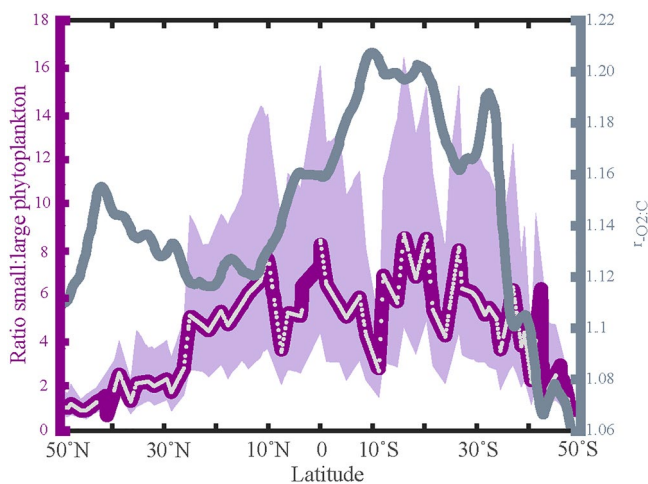


Figure 6. Relationship between cell size and the respiration quotient. Gray dots represent interpolated samples. The dark purple line is a smooth 6-point moving average representing the average of all Monte Carlo runs. The light purple shaded region represents a Monte Carlo analysis (95% confidence interval for $n = 1,000$). The gray line represents a smooth 48-point moving average of measured $r_{O_2:C}$.

from the equatorial Pacific and Arabian Sea (Hedges et al., 2001). Here, the lipid content either decreased or increased with depth indicating that processing of POM can affect the macromolecular composition and $r_{-O_2:C}$. Thus, reprocessing of organic material may lead to divergent $r_{-O_2:C}$ but this process is currently difficult to constrain. While recognizing that more research is required, our observations support that the respiration quotient is primarily controlled by the meridional gradient in temperature, nutrient supply, and plankton size structure and secondarily by the spatial transition between N and P stress.

The respiration quotient shows diel shifts but with a low impact on the overall variance. In our Atlantic Ocean samples, we found that POC peaks in the evening at 21:00 whereas the PCOD peak is delayed by 2 hr. This lag results in a minimal yet statistically significant diel cycle. Two lines of evidence could explain why we observe a minimal cycle in $r_{-O_2:C}$. The first is cellular processing of biochemical components during times of stress. Under P stress, many small phytoplankton can substitute non-phosphorus membrane lipids for phospholipids (Martin et al., 2011; Van Mooy et al., 2009). Due to changes in nutrient stress regime over the Atlantic Ocean, transitioning from P to N stress, it is possible our analysis simply misses a stronger regional signal. The second line of evidence is the lower presence of eukaryotic phytoplankton during large sections of the Atlantic Transect. In the North Pacific Subtropical Gyre, storage lipids show a clear diel cycle in eukaryotic phytoplankton (Becker et al., 2018). Based on flow cytometry data collected during our Atlantic Ocean cruise, picoeukaryotes and nanoeukaryotes biomass was mostly below marine cyanobacteria (Figure 6). Thus, regions dominated by larger phytoplankton may result in stronger diel oscillation for $r_{-O_2:C}$.

Multiple caveats need to be considered within the framework of this study. First, our sampling design consisted of an hourly collection of non-replicated samples to increase the spatial and temporal resolution at the expense of replication (Lennon, 2011). In contrast, samples were taken every 4 hr, with triplicates of POC and sextuples of PCOD in the Pacific Ocean (Moreno et al., 2020). Although the un-replicated hourly sampling regime resulted in greater spatial and temporal coverage (e.g., for capturing diel variation), there is an increased variance between stations as seen in Figure 2c. Second, our nutrient stress biomarkers are based on *Prochlorococcus* gene profiles and may only partially represent the stress profile of the full plankton community (Ustick et al., 2021). The third caveat is that we were unable to directly measure specific biomolecules responsible for shifts in PCOD. Our third hypothesis describes a positive relationship whereby the respiration quotient increases with more storage lipid accumulation during N stress. Although studies have shown that both N and P stress can adjust lipid content, N stress produces higher concentrations of storage fatty acids (Converti et al., 2009; Juneja et al., 2013; Praveenkumar et al., 2012). As such, $r_{-O_2:C}$ ratios would increase due to more oxygen required for degrading lipid carbons, and we hope in future studies to directly quantify biomolecule concentrations to further test this hypothesis. Temperature has also been shown to influence the saturated and unsaturated fatty acid composition with different C oxidation states within microalgae (Converti et al., 2009; Thompson et al., 1992). Fatty acid (14:0) concentrations were found to increase ~20% when temperature increased by 15°C, whereas polyunsaturated fatty acids were consistently higher at low temperatures (Thompson et al., 1992). Therefore, although our results provide evidence for linking temperature changes and the respiration quotient, the secondary impact of nutrient limitation can result in additive or neutralizing variation. The final caveat is the blank corrections for either POC or PCOD measurements. Currently much research has been conducted to determine the best method for blank correction (Chaves et al., 2021; Novak et al., 2018; Turnewitsch et al., 2007). However, no standard method has yet to be determined. Using one potential method, regression-based blanking, we have estimated the O₂ concentration adsorbed to our filters as ~1 μmol (less than 5% of observed PCOD concentrations). However, our POC and PCOD samples are taken in tangent, so we expect the variation in DOM adsorbed to be minimal. Nevertheless, our findings provide the first measurements needed to test and determine the impact of each the proposed four mechanisms on $r_{-O_2:C}$ variability.

Future changes to sea- surface temperature and nutrient availability could affect the biological regulation of the respiration quotient and in turn, deep ocean oxygen demand. Given near certain future rising surface ocean temperature (Durack et al., 2018; Kwiatkowski et al., 2020), our data suggests a higher $r_{-O_2:C}$ and biological oxygen demand (Moreno et al., 2020). However, future changes to nutrient stress and shifts between N and P limitation are less certain. The aeolian delivery of iron and associated stimulation of nitrogen fixation is an important lever for shifts between N and P limitation (Martiny et al., 2019; Ustick et al., 2021; Wu et al., 2000). However, future changes to both the total amount as well as regional distribution of ocean iron inputs are not well understood (Hamilton et al., 2019). It has been suggested that the Southern Hemisphere aeolian Fe flux could

increase by up to 80% (Hamilton et al., 2020) and stimulate both primary production and nitrogen fixation. In a biogeochemical model, increased delivery of Fe enhanced N stress in regions surrounding the eastern Pacific equatorial upwelling region (Hamilton et al., 2020). Another model study suggested that future N fixation would decrease globally, but changes to N versus P limitation were not identified (Wrightson & Tagliabue, 2020). As such, an expansion of N-limited regions would amplify $r_{-O_2:C}$, whereas increased P limitation would dampen the warming effect on the respiration quotient. However, it is unknown whether such nutrient limitation changes will occur. Overall, our findings emphasize how biological processes lead to complex interactions between the carbon, oxygen, and nutrient cycles with important implications for future ocean environmental conditions.

Conflict of Interest

The authors declare no conflicts of interest relevant to this study.

Data Availability Statement

Particulate organic matter data and metadata that support the findings are available through <http://cchdo.ucsd.edu> (<https://cchdo.ucsd.edu/cruise/74JC20180923>) and BCO-DMO project 2178 (<https://www.bco-dmo.org/project/2178>). Particulate chemical oxygen demand data have been deposited in the National Oceanography Centre British Oceanographic Data Centre as cited: Moreno et al. (2022, <https://doi.org/10.5285/D76D90BB-5D7A-5415-E053-6C86ABC0D182>).

References

- Altabet, M. A. (2007). Constraints on oceanic N balance/imbalance from sedimentary 15N records. *Biogeosciences*, 4(1), 75–86. <https://doi.org/10.5194/bg-4-75-2007>
- Anderson, L. A. (1995). On the hydrogen and oxygen content of marine phytoplankton. *Deep Sea Research Part I: Oceanographic Research Papers*, 42(9), 1675–1680. [https://doi.org/10.1016/0967-0637\(95\)00072-E](https://doi.org/10.1016/0967-0637(95)00072-E)
- Becker, K. W., Collins, J. R., Durham, B. P., Groussman, R. D., White, A. E., Fredricks, H. F., et al. (2018). Daily changes in phytoplankton lipidomes reveal mechanisms of energy storage in the open ocean. *Nature Communications*, 9(1), 5179. <https://doi.org/10.1038/s41467-018-07346-z>
- Bopp, L., Resplandy, L., Orr, J. C., Doney, S. C., Dunne, J. P., Gehlen, M., et al. (2013). Multiple stressors of ocean ecosystems in the 21st century: Projections with CMIP5 models. *Biogeosciences*, 10(10), 6225–6245. <https://doi.org/10.5194/bg-10-6225-2013>
- Casey, J. R., Aucan, J. P., Goldberg, S. R., & Lomas, M. W. (2013). Changes in partitioning of carbon amongst photosynthetic pico- and nano-plankton groups in the Sargasso Sea in response to changes in the North Atlantic Oscillation. *Deep-Sea Research Part II Topical Studies in Oceanography*, 93, 58–70. <https://doi.org/10.1016/j.dsr2.2013.02.002>
- Chaves, J. E., Cetinić, I., Dall'Olmo, G., Estapa, M., Gardner, W., Goñi, M., et al. (2021). Particulate organic matter sampling and measurement protocols: Consensus towards future ocean color missions. *IOCCG Protocol Series*, 6(August).
- Chen, Y., Tang, X., Kapoore, R. V., Xu, C., & Vaidyanathan, S. (2015). Influence of nutrient status on the accumulation of biomass and lipid in *Nannochloropsis salina* and *Dunaliella salina*. *Energy Conversion and Management*, 106, 61–72. <https://doi.org/10.1016/j.enconman.2015.09.025>
- Converti, A., Casazza, A. A., Ortiz, E. Y., Perego, P., & Del Borghi, M. (2009). Effect of temperature and nitrogen concentration on the growth and lipid content of *Nannochloropsis oculata* and *Chlorella vulgaris* for biodiesel production. *Chemical Engineering and Processing: Process Intensification*, 48(6), 1146–1151. <https://doi.org/10.1016/j.ccep.2009.03.006>
- DeVries, T., & Deutsch, C. (2014). Large-scale variations in the stoichiometry of marine organic matter respiration. *Nature Geoscience*, 7(12), 890–894. <https://doi.org/10.1038/ngeo2300>
- Durack, P. J., Gleckler, P. J., Purkey, S. G., Johnson, G. C., Lyman, J. M., & Boyer, T. P. (2018). Ocean warming: From the surface to the deep in observations and models. *Oceanography*, 31(2), 41–51. <https://doi.org/10.5670/oceanog.2018.227>
- Falkowski, P. G., Algeo, T., Codispoti, L., Deutsch, C. A., Emerson, S., Hales, B., et al. (2011). Ocean deoxygenation: Past, present, and future. *Eos, Transactions American Geophysical Union*, 92(46), 409–410. <https://doi.org/10.1038/nature21399>
- Finkel, Z. V., Follows, M. J., Liefer, J. D., Brown, C. M., Benner, I., & Irwin, A. J. (2016). Phylogenetic diversity in the macromolecular composition of microalgae. *PLoS One*, 11(5), e0155977. <https://doi.org/10.1371/journal.pone.0155977>
- Hamilton, D., Moore, J. K., Arnett, A., Bond, T. C., Carslaw, K. S., Hantson, S., et al. (2020). Impact of changes to the atmospheric soluble iron deposition flux on ocean biogeochemical cycles in the Anthropocene. *Global Biogeochemical Cycles*, 34(3), e2019GB006448. <https://doi.org/10.1029/2019gb006448>
- Hamilton, D., Scanza, R., Feng, Y., Guinness, J., Kok, J., Li, L., et al. (2019). Improved methodologies for Earth system modelling of atmospheric soluble iron and observation comparisons using the Mechanism of Intermediate complexity for Modelling Iron (MIMI v.1.0). *Geoscientific Model Development Discussions*, 1–54. <https://doi.org/10.5194/gmd-2019-84>
- Hedges, J. I., Baldock, J. A., Gelinás, Y., Lee, C., Peterson, M., & Wakeham, S. G. (2001). Evidence for non-selective preservation of organic matter in sinking marine particles. *Nature*, 409(6822), 801–804. <https://doi.org/10.1038/35057247>
- Illman, A. M., Scragg, A. H., & Shales, S. W. (2000). Increase in *Chlorella* strains calorific values when grown in low nitrogen medium. *Enzyme and Microbial Technology*, 27(8), 631–635. [https://doi.org/10.1016/S0141-0229\(00\)00266-0](https://doi.org/10.1016/S0141-0229(00)00266-0)
- Jiao, N., Herndl, G. J., Hansell, D. A., Benner, R., Kattner, G., Wilhelm, S. W., et al. (2010). Microbial production of recalcitrant dissolved organic matter: Long-term carbon storage in the global ocean. *Nature Reviews Microbiology*, 8(8), 593–599. <https://doi.org/10.1038/nrmicro2386>
- Juneja, A., Ceballos, R. M., & Murthy, G. S. (2013). Effects of environmental factors and nutrient availability on the biochemical composition of algae for biofuels production: A review. *Energies*, 6(9), 4607–4638. <https://doi.org/10.3390/en6094607>

- Kaiser, K., & Benner, R. (2008). Major bacterial contribution to the ocean reservoir of detrital organic carbon and nitrogen. *Limnology & Oceanography*, 53(3), 1192. <https://doi.org/10.4319/lo.2008.53.3.1192>
- Karl, D. M., & Grabowski, E. (2017). The importance of H in particulate organic matter stoichiometry, export and energy flow. *Frontiers in Microbiology*, 8(May), 1–7. <https://doi.org/10.3389/fmicb.2017.00826>
- Keeling, R. E., Körtzinger, A., & Gruber, N. (2010). Ocean deoxygenation in a warming world. *Annual Review of Marine Science*, 2(1), 199–229. <https://doi.org/10.1146/annurev.marine.010908.163855>
- Kwiatkowski, L., Torres, O., Bopp, L., Aumont, O., Chamberlain, M., Christian, J., et al. (2020). Twenty-first century ocean warming, acidification, deoxygenation, and upper ocean nutrient decline from CMIP6 model projections. *Biogeosciences Discussions*, 1–43. <https://doi.org/10.5194/bg-2020-16>
- Lennon, J. T. (2011). Replication, lies and lesser-known truths regarding experimental design in environmental microbiology. *Environmental Microbiology*, 13(6), 1383–1386. <https://doi.org/10.1111/j.1462-2920.2011.02445.x>
- Linacre, L. P., Landry, M. R., Lara-Lara, J. R., Hernández-Ayón, J. M., & Bazán-Guzmán, C. (2010). Picoplankton dynamics during contrasting seasonal oceanographic conditions at a coastal upwelling station off Northern Baja California, México. *Journal of Plankton Research*, 32(4), 539–557. <https://doi.org/10.1093/plankt/fbp148>
- Martin, P., Van Mooy, B. A. S., Heithoff, A., & Dyhrman, S. T. (2011). Phosphorus supply drives rapid turnover of membrane phospholipids in the diatom *Thalassiosira pseudonana*. *The ISME Journal*, 5(6), 1057–1060. <https://doi.org/10.1038/ismej.2010.192>
- Martiny, A. C., Lomas, M. W., Fu, W., Boyd, P. W., Chen, Y. L., Cutter, G. A., et al. (2019). Biogeochemical controls of surface ocean phosphate. *Science Advances*, 5(8), 1–10. <https://doi.org/10.1126/sciadv.aax0341>
- Matalana-Surget, S., Derock, J., Leroy, B., Badri, H., Deschoenmaeker, F., & Wattiez, R. (2014). Proteome-wide analysis and diel proteomic profiling of the cyanobacterium *Arthrospira platensis* PCC 8005. *PLoS One*, 9(6), e99076. <https://doi.org/10.1371/journal.pone.0099076>
- Mather, R. L., Reynolds, S. E., Wolff, G. A., Williams, R. G., Torres-Valdes, S., Woodward, E. M. S., et al. (2008). Phosphorus cycling in the North and South Atlantic Ocean subtropical gyres. *Nature Geoscience*, 1(7), 439–443. <https://doi.org/10.1038/ngeo232>
- Moore, C. M., Mills, M. M., Arrigo, K. R., Berman-Frank, I., Bopp, L., Boyd, P. W., et al. (2013). Processes and patterns of oceanic nutrient limitation. *Nature Geoscience*, 6(9), 701–710. <https://doi.org/10.1038/ngeo1765>
- Moreno, A. R., Garcia, C. A., Larkin, A. A., Lee, J. A., Wang, W.-L., Moore, J. K., et al. (2020). Latitudinal gradient in the respiration quotient and the implications for ocean oxygen availability. *Proceedings of the National Academy of Sciences*, 117(37), 22866–22872. <https://doi.org/10.1073/pnas.2004986117>
- Moreno, A. R., Larkin, A., Lee, J. A., Gerace, S. D., & Martiny, A. (2022). Surface ocean particulate chemical oxygen demand (PCOD) of organic matter (POM) from CTD and underway-collected samples along a north-south transect in the Atlantic Ocean on cruise AMT28 (JR18001). NERC EDS British Oceanographic Data Centre NOC. <https://doi.org/10.5285/d76d90bb-5d7a-5415-e053-6c86abc0d182>
- Novak, M. G., Cetinić, I., Chaves, J. E., & Mannino, A. (2018). The adsorption of dissolved organic carbon onto glass fiber filters and its effect on the measurement of particulate organic carbon: A laboratory and modeling exercise. *Limnology and Oceanography: Methods*, 16(6), 356–366. <https://doi.org/10.1002/lom3.10248>
- Praveenkumar, R., Shameera, K., Mahalakshmi, G., Akbarsha, M. A., & Thajuddin, N. (2012). Influence of nutrient deprivations on lipid accumulation in a dominant indigenous microalga *Chlorella* sp., BUM11008: Evaluation for biodiesel production. *Biomass and Bioenergy*, 37, 60–66. <https://doi.org/10.1016/j.biombioe.2011.12.035>
- Quay, P., Emerson, S., & Palevsky, H. (2020). Regional pattern of the ocean's biological pump based on geochemical observations. *Geophysical Research Letters*, 47(14), 1–10. <https://doi.org/10.1029/2020GL088098>
- Redfield, A. C. (1958). The biological control of the chemical factors in the environment. *American Scientist*, 46(3), 1–18.
- Reitan, K. I., Rainuzzo, J. R., & Olsen, Y. (1994). Effect of nutrient limitation of fatty acid and lipid content of marine microalgae. *Journal of Phycolgy*, 30(6), 972–979. <https://doi.org/10.1111/j.0022-3646.1994.00972.x>
- Reygondeau, G., Longhurst, A., Martinez, E., Beaugrand, G., Antoine, D., & Maury, O. (2013). Dynamic biogeochemical provinces in the global ocean. *Global Biogeochemical Cycles*, 27(4), 1046–1058. <https://doi.org/10.1002/gbc.20089>
- Robinson, C. (2019). Microbial respiration, the engine of ocean deoxygenation. *Frontiers in Marine Science*, 5(Jan), 1–13. <https://doi.org/10.3389/fmars.2018.00533>
- Schmidtko, S., Stramma, L., & Visbeck, M. (2017). Decline in global oceanic oxygen content during the past five decades. *Nature*, 542(7641), 335–339. <https://doi.org/10.1038/nature21399>
- Stramma, L., Johnson, G. C., Sprintall, J., & Mohrholz, V. (2008). Expanding oxygen-minimum zones in the tropical oceans. *Science*, 320(5876), 655–658. <https://doi.org/10.1126/science.1153847>
- Thompson, P. A., Guo, M.-X., Harrison, P. J., & Whyte, J. N. C. (1992). Effects of variation in temperature. II. On the fatty acid composition of eight species of marine phytoplankton. *Journal of Phycolgy*, 28(4), 488–497. <https://doi.org/10.1111/j.0022-3646.1992.00488.x>
- Turnewitsch, R., Springer, B. M., Kiriakoulakis, K., Vilas, J. C., Aristegui, J., Wolff, G., et al. (2007). Determination of particulate organic carbon (POC) in seawater: The relative methodological importance of artificial gains and losses in two glass-fiber-filter-based techniques. *Marine Chemistry*, 105(3–4), 208–228. <https://doi.org/10.1016/j.marchem.2007.01.017>
- Ustick, L. J., Larkin, A. A., Garcia, C. A., Garcia, N. S., Brock, M. L., Lee, J. A., et al. (2021). Metagenomic analysis reveals global-scale patterns of ocean nutrient limitation. *Science*, 372(6539), 287–291. <https://doi.org/10.1126/science.abe6301>
- Van Mooy, B. A. S., Benjamin, A. S., Rocap, G., Fredricks, H. F., Evans, C. T., & Devol, A. H. (2006). Sulfolipids dramatically decrease phosphorus demand by picocyanobacteria in oligotrophic marine environments. *Proceedings of the National Academy of Sciences of the United States of America*, 103(23), 8607–8612. <https://doi.org/10.1073/pnas.0600540103>
- Van Mooy, B. A. S., Fredricks, H. F., Pedler, B. E., Dyhrman, S. T., Karl, D. M., Koblizek, M., et al. (2009). Phytoplankton in the ocean use non-phosphorus lipids in response to phosphorus scarcity. *Nature*, 458(7234), 69–72. <https://doi.org/10.1038/nature07659>
- Van Mooy, B. A. S., Keil, R. G., & Devol, A. H. (2002). Impact of suboxia on sinking particulate organic carbon: Enhanced carbon flux and preferential degradation of amino acids via denitrification. *Geochimica et Cosmochimica Acta*, 66(3), 457–465. [https://doi.org/10.1016/S0016-7037\(01\)00787-6](https://doi.org/10.1016/S0016-7037(01)00787-6)
- Wakeham, S. G., Lee, C., Hedges, J. I., Hernes, P. J., & Peterson, M. L. (1997). Molecular indicators of diagenetic status in marine organic matter. *Geochimica et Cosmochimica Acta*, 61(24), 5363–5369. [https://doi.org/10.1016/S0016-7037\(97\)00312-8](https://doi.org/10.1016/S0016-7037(97)00312-8)
- Wrightson, L., & Tagliabue, A. (2020). Quantifying the impact of climate change on marine diazotrophy: Insights from Earth system models. *Frontiers in Marine Science*, 7(July), 1–9. <https://doi.org/10.3389/fmars.2020.00635>
- Wu, J., Sunda, W., Boyle, E. A., & Karl, D. M. (2000). Phosphate depletion in the Western North Atlantic Ocean. *Science*, 289(5480), 759–762. <https://doi.org/10.1126/science.289.5480.759>